Towards the growth of $Cu_2ZnSn_{1-x}Ge_xS_4$ thin films by a single-stage process: Effect of substrate temperature and composition

R. Caballero[a,*], J.M. Cano-Torres[a], E. Garcia-Llamas[a], X. Fontané[b], A. Pérez-Rodríguez[b,c], D. Greiner[d], C.A. Kaufmann[d], J.M. Merino[a], I. Victorov[e], G. Baraldi[f], M. Valakh[g], I. Bodnar[e], V. Izquierdo-Roca[b], M. León[a]

[a]Universidad Autónoma de Madrid, Departamento de Física Aplicada, C/ Francisco Tomás y Valiente 7, 28049 Madrid, Spain

[b]IREC, Catalonia Institute for Energy Research, C. Jardins de les Dones de Negre 1, Sant Adriá del Besòs, 08930 Barcelona, Spain

[c]IN_2UB, Department d´Electrónica, Universitat de Barcelona, C. Martí I Franquès 1, 08028 Barcelona, Spain

[d]Helmholtz Zentrum Berlin für Materialien und Energie, Hahn-Meitner Platz 1, 14109 Berlin, Germany

[e]Belarusian State University of Informatics and Radioelectronics, P. Brovska 6, 220013 Minsk, Belarus

[f]Instituto de Óptica Daza de Valdés, CSIC, C/ Serrano 121, 28006 Madrid, Spain

[g]V. Lashkaryov Institute of Semiconductor Physics of National Academy of Sciences of Ukraine, 41 Prospect Nauky, 03028 Kyiv, Ukraine

*Corresponding author. Tel: +34 914978559; Fax: +34 914973969

E-mail address: raquel.caballero@uam.es (R. Caballero)

Abstract

$Cu_2ZnSn_{1-x}Ge_xS_4$ (CZTGS) thin films prepared by flash evaporation of a Zn-rich $Cu_2ZnSn_{0.5}Ge_{0.5}S_4$ bulk compound in powder form, and a subsequent thermal annealing in S containing Ar atmosphere are studied. The effect of the substrate temperature during evaporation and the initial composition of the precursor powder on the growth mechanism and properties of the final CZTGS thin film are investigated. The microstructure of the films and elemental depth profiles depend strongly on the growth conditions used. Incorporation of Ge into the Cu_2ZnSnS_4 lattice is demonstrated by the shift of the relevant X-ray diffraction peaks and Raman vibrational modes towards higher diffraction angles and frequencies respectively. A Raman mode at around 348-

351 cm^{-1} is identified as characteristic of CZTGS alloys for x = [Ge]/([Sn]+[Ge]) = 0.14-0.30. The supply of Ge enables the reduction of the Sn loss via a saccrifical Ge loss. This fact allows increasing the substrate temperature up to 350º C during the evaporation, forming a high quality kesterite material and therefore, reducing the deposition process to one single stage.

Keywords: CZTGS, Germanium, Earth abundant, thin film, solar cells

1. Introduction

$Cu_2ZnSn(S,Se)_4$ (CZTSSe) kesterite material is an excellent candidate to be used as absorber layer for thin-film solar cells. This is because this earth-abundant material presents *p*-type conductivity, a high absorption coefficient and direct band gap energy from 1.0 to 1.5 *e*V depending on the anions' ratio [1]. Nowadays, a top efficiency of 12.6 % has been achieved [2]. However, it is still quite low compared to the 21.7 % efficiency reported for $Cu(In,Ga)Se_2$ (CIGSe) solar cells [3]. One of the key factors to realize this high performance in CIGSe devices is the Ga/In substitution, leading to band gap tuning. As previously reported [4-6], a similar band gap grading is possible to be achieved with the partial substitution of tin with germanium in the CZTSSe lattice. As a further example also Guo [4] and Hages [7] et al. have reported an enhanced performance of CZTSSe devices with the addition of Ge. Tandem photovoltaic devices allow light harvesting of a broader part of the light spectrum . Recently, Todorov et al. [8] have demonstrated the potential of a monolithic CZTSSe-perovskite architecture as multijuncion device. Hence the possibility of tuning the band gap energy and improving the device performance by adding Ge makes this material suitable and attractive to be used for a tandem solar cell device.

On the other hand, it is still necessary to understand the role of the growth parameters to produce kesterite material with the optimum properties for maximum device efficiency. Cu_2ZnSnS_4 (CZTS), $Cu_2ZnSnSe_4$ (CZTSe) and CZTSSe thin films have been synthesized via different techniques: thermal evaporation [9-10], co-evaporation [11-12], sputtering [13-14], sol-gel [15], electroplating [16], etc. Many of them have been fabricated by a sequential, or two-stage, process: deposition of precursor followed by post-sulfurization/selenization. This is advantageous due to its capability and high throughput. However, it is also desirable to reduce the number of stages during the growth process.

Here, $Cu_2ZnSn_{1-x}Ge_xS_4$ (CZTGS) (x = [Ge]/([Sn]+[Ge]) thin films have been grown by flash evaporation and subsequent annealing under Ar atmosphere. Different deposition parameters, such as substrate temperature during the evaporation, Ar pressure, temperature and time during the annealing have been studied. The goal of the present work is to investigate the effect of the growth parameters on the distribution of the elements, structural, morphological and optical properties of the alloy compound. We show that the increased substrate temperature of up to 350º C during the evaporation can produce quality kesterite material by a single-stage process. The addition of Ge makes possible the reduction of Sn loss via an increased sacrifical loss of germanium.

2. Experimental

A Zn-rich $Cu_2ZnSn_{0.5}Ge_{0.5}S_4$ compound was synthesized by a modified Bridgman method [17]. This compound was first ground to a powder and then used as source material for evaporation. CZTGS thin films were fabricated by a sequential, or two-stage, process: evaporation followed by a thermal treatment. In the first stage, CZTGS thin films were deposited by flash evaporation [18] onto Mo coated glass and glass substrates using the compound in powder form at nominal substrate temperatures, T_{substr} of 100º and 350º C. As previously reported [19], a preferential re-evaporation of Zn takes place during the flash evaporation process, leading to Zn-poor thin films. It was reported that, despite a Zn-rich precursor powder, a significantly decreased Zn-content was obtained after evaporation. This behavior was related to the high partial vapor pressure of Zn. Throughout the paper, Flash 1 refers to the evaporation process performed at T_{substr} = 100º C. In addition, a precursor with excess of ZnS was prepared by two more deposition procedures: Flash 2 at T_{substr} = 100º C and Flash 3 at T_{substr} = 350º C. Table 1 summarizes the different deposition processes carried out and the composition of the thin films and the bulk compound. The composition was measured by Energy Dispersive X-ray spectroscopy (EDX) (Oxford instruments, model INCAx-sight) inside a Hitachi S-3000N scanning electron microscope (SEM). EDX measurements were carried out at 25 kV operating voltage, and the Cu K, Zn K, Ge K, Sn L and S K lines were used for quantification. The second stage of the process consisted of a thermal treatment of the samples in Ar atmosphere (at pressures of 4.5 x 10^4 and 9.5 x 10^4 Pa) under excess of elemental S. For that purpose, the as-evaporated thin films were placed in a partially closed graphite box, of 56 mm x 70 mm x 20.5 mm with a hole

of 1 mm diameter in the lid, and inserted into a quartz tube furnace. The samples size was of 100 mm^2 approximately. In order to have an overpressure of S, 30 mg of elemental sulfur were also placed inside the graphite container next to the substrate. The maximum S overpressure was of 2.15 x 10^5 Pa at 550º C and of 1.20 x 10^5 Pa at 500º C. The heating and cooling rates were 20º C/min and 10º C/min respectively. Parameters such as maximum temperature, Ar pressure and time at the maximum temperature were varied to obtain the CZTGS material with the optimum properties. The composition of the annealed samples and the details of the thermal treatments applied are collected in Table 2. The samples coming from the process Flash 1 are characterized by a low Zn content; those from Flash 2 by a significantly decreased Cu and increased Zn concentrations and the samples from process Flash 3 by a near-ideal composition for photovoltaic applications, i.e. Cu-poor and Zn-rich.

Grazing incidence X-ray diffraction (GIXRD) was performed to investigate the structural properties of the CZTGS thin films. GIXRD data were collected with a PaNAlytical X´Pert Pro MPD diffractometer, using Cu K_α radiation and a multilayer mirror. Detector scans with incident angles of 0.25º, 2º and 4º were carried out. Micro Raman spectra were obtained at room temperature in a Horiba Jobin Ivon T64000 spectrometer. The laser wavelength was adjusted to 514.5 nm with a spot size of 1.25 μm diameter. The samples from flash evaporation 3 were measured using a 532 nm excitation wavelength. Moreover, Raman scattering measurements at 325 nm were carried out to enhance the detection sensibility to the potential presence of ZnS phases [20]. 532 and 325 nm Raman scattering measurements were performed in back scattering configuration with LabRam HR800-UV Horiba-Jobin Yvon spectrometer coupled to an Olympus metallographic microscope. The laser spot diameter in both cases has been estimated to be in the order of 1 μm and the power density on the surface of the samples was kept around 50 W/cm^2. To avoid effects in the spectra related to potential microscopic inhomogeneities, the spot was rastered over an area of 30 x 30 μm^2 for both excitations wavelengths. The first-order Raman spectrum of Si single crystal was measured as a reference, and the spectra were corrected with respect to the Si line at 520 cm^{-1}. Both spectrometers gave us almost identical Raman spectra when working at 514.5 nm and 532 nm.

Scanning electron microscopy was used to study the morphology of the CZTGS/Mo/glass structure using a Philips XL30S FEG scanning electron microscope at

10 kV operating voltage. Glow discharge optical emission spectroscopy (GDOES) with a Spectruma GDA 650 was performed in pulsed RF mode to study the elemental depth profile through the CZTGS layer. Argon plasma with a pulsed RF mode was used to sputter the CZTGS and Mo layer and radiation from the ionized atoms from the layer is detected with a CCD array. Cross-sectional EDX mapping was conducted on a LEO GEMINI 1530 SEM (Carl Zeiss AG, Oberkochen, Germany) and a Thermo Fisher silicon-drift X-ray detector (Thermo Fisher Company, Dreiecich, Germany).

3. Results and discussion

3.1. As-evaporated CZTGS thin films

Table 1 shows a higher Zn concentration when a 50 atomic % excess of ZnS was added to the precursor synthesis. This leads to an atomic ratio of [Zn]/([Sn]+[Ge]) higher than 1, which is necessary to achieve high efficiency solar cells [21]. A decreased Ge concentration is observed when the substrate temperature is increased, as also reported by Guo et al. [4]. While an atomic ratio x = [Ge]/([Sn]+[Ge]) of ~ 0.5 is maintained for the evaporation processes 1 and 2, x is drastically reduced when a substrate temperature of 350º C is used. This can be related to the high vapour pressure of Ge sulfides [22].

Figure 1 presents the GIXRD (GI = 4º) spectra of the as-evaporated thin films. The JCPDS data for tetragonal Cu_2ZnSnS_4 (No. 01-075-4122), tetragonal Cu_2ZnGeS_4 (CZGS) (No. 04-012-7580), hexagonal wurtzite ZnS (No. 00-012-0688) and cubic Cu_2S (No. 00-053-0522) are also shown. Inset of Figure 1 shows the 112 and 200/204 diffraction peaks. Two features can be distinguished here. First, the diffraction peaks are shifted towards higher diffraction angles for increased Ge concentrations. This fact is explained by the replacement of large Sn atoms by smaller Ge atoms, which leads to smaller lattice parameters. These spectra reveal the incorporation of Ge into the lattice. Secondly, the higher substrate temperature of 350º C leads to an enhanced crystallinity and the presence of the main peaks corresponding to the CZTGS alloy material are observed (see as-evaporated sample of process Flash 3). However, it is quite difficult to rule out the presence of secondary phases such as ZnS and Cu-S due to the closeness of the diffraction peaks of these phases with those of CZTS.

3.2. CZTGS after thermal treatment in Ar atmosphere

3.2.1. CZTGS thin films coming from evaporation process Flash 1

GIXRD spectra of the samples corresponding to the first evaporation process after different thermal treatments are displayed in Figure 2. In all of them, the diffraction peaks are located between those of tetragonal CZTS and CZGS compounds. Moreover, SnS (JCPDS No. 39-0354) is also identified for the samples with atomic ratio [Zn]/([Sn] + [Ge]) ≤ 0.74. It has been reported a Sn loss when annealing CZTS thin films at high temperatures due to the high partial pressure of SnS [23]. We previously detected increased Cu and Zn concentrations after the sulfurization process because of the Sn loss in the case of Cu_2ZnSnS_4 thin films [19]. However, here a significant loss of Ge takes place, without observing a decrease in the Sn content. From the literature, GeS has a much higher vapor pressure than SnS at 550º C [24-25]. As suggested by Chen et al. [21], sublimation of Ge sulfides (GeS/GeS_2) can be assumed during the sulfurization process inducing Ge loss. Loss of Ge seems to be reduced by using a lower Ar pressure for 30 minutes during the sulfurization process.

Figure 3 displays Raman spectra of the samples under excitation using light with a wavelength of 514.5 nm, including fits with Lorentzian curves. These show several weak peaks with two dominant peaks at 290 cm^{-1} and 340 cm^{-1}. This fingerprint contrasts with the Raman spectra reported for the wurtzstannite CZGS semiconductor at non-resonant conditions [26]. The Raman spectrum of wurtzstannite CZGS is only dominated by a band at 362 cm^{-1}. On the other hand, the spectra of Figure 3 show a high similarity to the fingerprint of the kesterite CZTS [27], suggesting that these samples present the same kesterite structure. The slight red shift of the dominant bands with respect to the A modes reported by [27-28] (287 cm^{-1} and 338 cm^{-1}) is assigned to the Ge incorporation in the Sn sites. As shown in [5], $Cu_2ZnSn_{0.9}Ge_{0.1}S_4$ single crystals presented the A mode at 339 cm^{-1}. Therefore, the mode at 340 cm^{-1} suggests a [Ge]/([Sn]+[Ge]) atomic ratio slightly higher than 0.1, which is in the case here .

The nature of the peak at 348-349 cm^{-1}, following from Lorentzian fits of the most intense A-band and particularly strong for the sample after TT3, should be discussed. There are two possible interpretations of this peak. This can be an E / B mode, manifested in pure CZTS at 347cm^{-1} as shown in [29]. However, it is more likely that this peak can be interpreted as CZGS-like A-mode of the mixed crystal CZTGS. Our preliminary results on the Raman scattering for several mixed CZTGS compounds [5] have shown that this solid solution is characterized by the so-called “two-mode rearrangement” of the phonon spectrum (at least for the most intense A-modes). In this

case, the Raman spectra of films of an intermediate compositions simultaneously modes of both components exist (CZTS and CZGS), and a change in composition is accompanied by redistribution of their relative intensities with only small frequency shifts. The most intensive A-phonon peak for CZGS has been reported at 360-362 cm^{-1} [26, 30]. With decreasing of Ge content in mixed CZTGS, that peak gradually shifts to lower frequencies by about 1 cm^{-1} with the composition change on 10%. This interpretation is supported by the fact that on Figure 3, the peak at 349 cm^{-1} is most clearly manifested in the sample after TT3, for which the content of Ge is 1.5 times more than in the samples after thermal treatments TT1 and TT4 (see Table 2).

Additionally the Raman measurements under green light excitation do not show bands that could be assigned to the Sn-S and Cu-S secondary. Two ways can explain this discrepancy with the SnS detection by GIXRD. First, the concentration of SnS phase may not be located at the surface. The Raman penetration depth under this condition is estimated to below 100 nm and the GI(4º)XRD gives us deeper information. The second possible explanation is possibly a concentration below the Raman detection limit.

No significant differences have been observed for samples annealed at different Ar pressures at 550º C for 30 minutes. However, a longer annealing time of 60 minutes, at the maximum temperature (TT4), shows a different Raman spectrum. A Raman peak at around 317-319 cm^{-1}, almost coinciding with the peak in the Raman spectra of CZTS [31], is observed for the samples after TT1 and TT3. However, this peak is absent in the sample after TT4. This fact can be associated with a lower crystalline perfection of the first two samples compared to the last one (such phenomena is known as "defect induced scattering"). This is supported by a smaller half-width and higher intensity of both A-peaks (290 and 340 cm^{-1}) in the spectrum of the sample TT4 (see inset of Figure 3.c.) and it has been reported for spectra of samples with low crystal quality [28].

In addition, Raman spectra were measured by using 325 nm excitation wavelength to confirm the nature of the mode at around 348-349 cm^{-1} (inset of Figure 3.b.). As reported in [20], ZnS is characterized by a main vibrational mode at around 350 cm^{-1} (LO peak) due to the existence of resonant excitation conditions that lead to an increase in the efficiency of this ZnS mode at this frequency. Moreover, a peak at 695 cm^{-1} (LO2 peak) appears, which has been identified as a second order band from ZnS. However, only some residual ZnS can be detected, which agrees with the composition of these thin films.

Figure 4.a.-4.d. show the cross-sectional SEM micrographs and the surface of the samples coming from the evaporation process Flash 1 after different thermal treatments. All of them are characterized by a columnar structure and grain size of the order of the film thickness. The higher Zn content obtained by a longer annealing time seems to reduce the grain size of the surface slightly. Zhang et al. [32] observed a grain size for CZTS thin films deposited by sol-gel after sulfurization at 0.04 MPa larger than that of CZTS thin films sulfurized at 0.1 MPa under a mixed Ar and sulfur vapor atmosphere. Here, no significant changes in the grain size are detected for different Ar pressures and annealing times used.

GDOES depth profiles of the samples of Figure 3 are displayed in Figure 5. Na diffuses from the glass towards the CZTGS surface, as for CIGSe solar cells [33]. The positive influence of Na on the CIGSe-based photovoltaic devices, generally via increased FF and V_{oc} [34], has been extensively reported together with the importance of controlling the addition of alkaline material to the absorber accurately [35]. Recently, the effect of Na on kesterite solar cells is being investigated, also observing an enhanced efficiency of the devices [36- 38]. Therefore, Na is an important parameter to control. Here, the Na profile is modified by the thermal treatment applied. A double Sn-gradient is observed for the samples after thermal treatments TT1 and TT3. A much higher Sn concentration next to the Mo back contact is detected for the sample annealed at lower Ar pressure (TT3). A drop of the Sn and a slightly increased Ge GDOES signal are observed near the front half of the CZTGS layer. The lower Ar pressure for a shorter sulfurization time led to a much higher S signal at the surface. As shown in Figure 2, a SnS phase is observed by GI(4º)XRD for both samples, after TT1 and TT3. The much higher Sn and S concentrations near the Mo layer could explain the higher intensity of the SnS diffraction peak at 31.9º for the sample after TT3. Moreover, no SnS is identified by GIXRD for the sample annealed for 1 h (TT4). That sample, TT4, is characterized by a much more uniform distribution of all the elements, especially of Sn and S. The longer annealing time at 550º C leads to a better diffusion of the elements to potentially form the pseudo-quaternary compound.

The ability to adjust the optical band gap energy of the absorber layer is critical for optimizing the performance of photovoltaic devices. The success of $Cu(In,Ga)Se_2$ solar cells is mainly based on the absorber band gap engineering [39]. A Ga gradient through the absorber layer has been shown to be a key issue to enhance the photovoltaic

parameters of CIGSe cells [40]. A similar strategy can be applied to the CZTSSe material by alloying with Ge. As shown in Figure 5, the distribution of Sn(Ge) through the CZTGS film can be modified by the thermal treatment applied. According to theoretical calculations for the electronic band structure of kesterites done by Persson [41], the estimated energy for CZTS of the Γ1 point (band gap energy, E_g) is 1.47 *e*V. A fundamental E_g of 1.59 *e*V and 1.95 *e*V was determined for $Cu_2ZnSn_{0.9}Ge_{0.1}S_4$ and $Cu_2ZnSn_{0.5}Ge_{0.5}S_4$ kesterite single crystals respectively by spectroscopic ellipsometry [5]. The band gap energy of the sample after TT4 was determined from transmittance and reflectance measurements and a value of 1.61 *e*V was obtained. The stannite-type material presents a higher band gap than the kesterite-type CZTGS [42]. According to the experimental E_g values obtained here, it is most likely that they show a dominant kesterite structure, in agreement with Raman spectroscopy measurements.

3.2.2 CZTGS thin films evaporated with a ZnS excess (Flash 2 and Flash 3)

The different thermal treatments applied to the samples from experiment Flash 1 evaporated at T_{substr}=100º C were not enough to achieve an atomic ratio of [Zn]/[IV] > 1. Therefore, new samples were evaporated at the same substrate temperature, adding an extra 50 atomic % of ZnS in the powder precursor (Flash 2). As shown in Table 1, a [Zn]/[IV] > 1 could now be achieved. However, the increased Zn concentration led to a significantly decreased Cu content after flash evaporation. Annealing of such samples resulted in atomic ratios: [Zn]/[IV] > 1 with Cu/([Zn] + [IV]) around 0.7; Cu-poor and Zn-rich films. High efficiency devices based on CZTSSe films are typically prepared under Zn-rich conditions, and this imposed Zn-excess may lead to the formation of ZnS as a secondary phase [9, 19]. GIXRD spectra of the Zn-richer sample after TT1 measured using different grazing incidence angles, show the characteristic peaks of the CZTGS material. However, the presence of ZnS cannot be ruled out at different penetration depths (see Figure 6.a.) so far. Raman spectroscopy performed using ZnS resonant conditions (325 nm) confirm the formation of ZnS phase [20]. Under these conditions a penetration depth of 25 nm is expected. Only ZnS is detected on the surface by Raman as shown in Figure 6.b., which displays the different Raman peaks associated to ZnS. The LO peak (close to 347 cm^{-1}) is strongly enhanced under UV conditions. Second and third order peaks of each of these modes are also observed (LO2 and LO3) at 695-697 and 1043-1045 cm^{-1} respectively. Additionally, small peaks at

273-276 cm^{-1} (T2(TO)) and 416 cm^{-1} (second order TO+LA and LO+TA modes) are detected. The broad bands centered around 635 and 978 cm^{-1} are higher order combinations of theses fundamental modes. Following Fairbrother´s model [43], we can expect a bigger ZnS grain size for the sample annealed at 550º C for 1 hour (TT2) because of the lower Raman shift of the modes. Meanwhile the first order peak is at 348.1 cm^{-1} for the sample annealed at 500º C for 30 min (TT5), the first order is at 346.9 cm^{-1} for the sample after TT2 (see inset of Figure 6.c.). As the grain size increases, the corresponding band gap energies are lower, and the free exciton energy shifts further away from the excitation energy, leading to increased enhancement of the LO2 and LO3 peaks. Figure 6.c. shows the area ratios of LO/LO2 and LO/LO3. The smallest area ratio LO/LO2 and LO/LO3 is an indication of the reduction of the quantum confinement effects that is in agreement with an increase ZnS grain size for the sample annealed at higher temperatures for longer time. However, ZnS segregation is a well-known problem for the formation of CZTSSe absorbers. This segregation has been believed to cause high series resistance [42]. It is possible to remove superficial ZnS secondary phase by HCl-based etching [44].

Cross-sectional SEM micrographs and the surface morphology of this series of samples show large grains together with other smaller crystals, which can be identified as ZnS (see Figure 4.e. - 4.h.). Inset of Figure 4.f. – 4.h. mainly shows the smaller grains on the surface related to the ZnS phase. EDX mappings reveal the primary presence of Zn in the smaller grains next to the Mo back contact as shown in Figure 4.j. for the sample annealed for 1 h. Therefore, there was not only an excess of Zn on the surface, but also inside the film. Kato et al. [10] found that while the ZnS is hardly controlled by varying precursor composition, the sulfurization conditions and precursor stacking are efficient. In [10], they also observed that the ZnS segregation at the backside of the absorber could have beneficial effects such as a back surface field. Here, it is observed that the composition of the precursor used for the evaporation is critical to controlling the ZnS phase formation. Even a sulfurization process carried out at 550º C for 4 hours led to quite Zn-rich samples.

On the other hand, the thermal treatment at the lower temperature of 500º C (TT5) shows the temperature as the parameter that plays the most important role with respect to the Ge loss. The sample annealed at 500º C is characterized by smaller grain sizes

due to the lower temperature used. This way, it was not possible to achieve the absorber layer with the proper composition for solar cells.

It is interesting to know what happens when the substrate temperature during the flash evaporation is increased. The samples evaporated at a substrate temperature of 350º C and an extra 50 atomic % of ZnS in the powder precursor, Flash 3, are characterized by a much lower Ge concentration. These as-evaporated films show a high crystallinity similar to that of the annealed samples and all the characteristic peaks of the CZTGS alloy, as presented in Figure 7.a. The different thermal treatments of such samples do not modify the material properties significantly. These results suggest that the evaporation at higher temperature produces the complete reaction to form high quality kesterite material. Different from the behaviour observed for the annealed samples coming from processes Flash 1 and 2, lower Cu and Zn concentrations and higher Ge contents are now obtained after thermal treatments. This can be related to the fact that the samples were already crystalline before annealing and the effect of the thermal treatment is entirely different. The composition of the sample annealed at 500º C corresponds to that typically reported to produce high efficiency solar cells. However, a Cu_2S secondary phase is identified by GIXRD for the sample before annealing and after annealing at 500º C .

Raman spectra measured at 532 nm of the samples shown in Figure 7.a. are displayed in Figure 7.b. In addition to the two main A symmetry modes at 291 cm^{-1} and 341 cm^{-1} of the kesterite phase, a new intense and well resolved Raman peak at 351 cm^{-1} is observed. In [5], a Raman mode at 354 cm^{-1} was detected for a $Cu_2ZnSn_{0.5}Ge_{0.5}S_4$ single crystal. Therefore, this newly resolved peak is due to the CZTGS with *x* near or equal to 0.3, in agreement with the thin films composition. The samples of Figure 3 do not show this Raman mode at 351 cm^{-1}, but a non-resolved contribution at 348-349 cm^{-1}. This is because of the lower [Ge]/([Sn]+[Ge]) atomic ratio for the samples coming from Flash 1. A small vibration mode at around 473-474 cm^{-1} can be identified as belonging to the $Cu_{2-y}S$ phase for the as-evaporated sample and after TT5 in agreement with GIXRD measurements. Raman spectra measured using 325 nm excitation wavelength suggest the formation of the ZnS phase on the surface (see Figure 7.c.). However, the concentration of ZnS is now much lower than that observed for the samples displayed in Figure 6. The LO/LO2 and A-CZTGS/LO-ZnS area ratios indicate that the ZnS grain size is around 10-20 nm [42] and of low concentration of ZnS.

Cross-sectional SEM micrographs and the surface morphology of CZTGS thin films show that the annealed-samples coming from the evaporation process Flash 3 present smaller grain sizes than those coming from Flash 1 (see Figure 4). This is related to the different growth mechanisms due to the different composition of the precursor compound as cause by the nominal substrate temperatures used during the flash evaporation. The samples from Flash 1 are Sn-richer, being Sn the largest atom in the system. It is well known that bigger grains do not imply better device performance for CIGSe solar cells [45]. Generally, it has been observed that larger grains improve the CZTS device performance. However, as mentioned above, the higher kesterite solar cell efficiencies are obtained for Cu-poor and Zn-rich composition.

On the other hand, the band gap energy of the samples after TT3 and TT5, determined from transmittance and reflectance measurements, are of 1.74 *e*V and 1.77 *e*V respectively. These values are in agreement with those reported for $Cu_2ZnSn_{1-x}Ge_xS_4$ single crystals with x =0.1 and 0.5 and E_g = 1.59 and 1.95 *e*V respectively [5]. The highest E_g for the sample annealed at lower temperature may be related to the presence of $Cu_{2-y}S$.

From the structural point of view, the quality of the as-evaporated samples at 350º C is as high as that obtained after annealing at 500-550º C. The results suggest that the crystallization of the kesterite takes already place at 350º C. This fact will allow reducing the stages of the growth of quality kesterite material.

Conclusions

$Cu_2ZnSn_{1-x}Ge_xS_4$ thin films with different compositions have been grown by flash evaporation followed by annealing in S containing Ar atmosphere. From our experimental observations, some aspects are here presented:

i) The incorporation of Ge into the CZTS lattice is demonstrated by the shift of the diffraction peaks and vibration modes towards higher diffraction angles and frequencies respectively. New Raman modes at around 348-351 cm^{-1} are observed when Sn is gradually replaced by Ge (x = 0.14 – 0.30), which correspond to CZTGS. Moreover, the incorporation of Ge is also confirmed by an increased band gap energy when the Ge content is higher.

ii) Ge loss is more significant at higher temperature and more important than the Sn loss during the post-sulfurization due to the higher vapour pressure of Ge sulfides than Sn

sulfides. The sublimation of GeS/GeS_2 is probably the route for Ge loss during the annealing.

iii) The microstructure of the samples depends strongly on the growth conditions of the kesterite layer and the composition of the compound.

iv) The composition of the initial precursor material for flash evaporation and the substrate temperature during the evaporation are the main parameters for the formation of different phases as determined by X-ray diffraction and Raman spectroscopy.

v) The sulfurization process can modify the elemental distribution through the whole kesterite layer, specially those of Sn, Ge, S and Na. Na diffusion from the glass substrate towards the CZTGS surface is observed, similar to the CIGSe solar cells.

vi) CZTGS thin films evaporated at a substrate temperature of 350º C present a structural quality as high as that after the annealing. Complete crystallization of the kesterite took place at T_{substr} = 350º C.

Quality kesterite thin films have been grown by a single-stage flash evaporation process via the addition of Ge, which enables the reduction of Sn loss during evaporation at a substrate temperature of 350º C.

Acknowledgements

RC acknowledges financial support from Spanish MINECO within the Ramón y Cajal programme (RYC-2011-08521) and VIR for the Juan de la Cierva fellowship (JCI-2011-10782). GB also acknowledges the CSIC-JAE pre-doctoral program, co-funded by the European Social Fund. This work was supported by the Marie Curie-IRSES project (PVICOKEST, GA: 269167), Marie Curie-ITN project (KESTCELL, GA: 316488), DAAD project (INTERKEST, Ref: 57050358), and MINECO projects (SUNBEAM, ENE2013-49136-C4-3-R) (TEC2012-38901-C02-01). A. Scheu is acknowledged for GDOES measurements.

References

[1] S. Chen, A. Walsh, J.H. yang, X.G. Gong, L. Sun, P.X. Yang, J.H. Chu, S.H. Wei, Compositional dependence of structural and electronic properties of $Cu_2ZnSn(S,Se)_4$ alloys for thin film solar cells, Phys. Rev. B 83 (2011) 125201-1-125201-5 (5 pages).

[2] W. Wang, M.T. Winkler, O. Gunawan, T. Gokmen, T.K. Todorov, Y. Zhu, D.B. Mitzi, Device characteristics of CZTSSe thin-film solar cells with 12.6% efficiency, Adv. Energy Mater. 4 (2014) 1301465-1-1301465-5 (5 pages).

[3] Press release, September 2014, http://www.zsw-bw.de/en/support/news.html

[4] Q. Guo, G.M. Ford, W.C. Yang, C.J. Hages, H.W. Hillhouse, R. Agrawal, Enhancing the performance of CZTSSe solar cells with Ge alloying, Sol. Energy Mater. Sol. Cells 105 (2012) 132-136.

[5] R. Caballero, I. Victorov, R. Serna, J.M. Cano-Torres, C. Maffiotte, E. Garcia-Llamas, J.M. Merino, M. Valakh, I. Bodnar, M. León, Band-gap engineering of $Cu_2ZnSn_{1-x}Ge_xS_4$ single crystals and influence of the surface properties, Acta Mater. 79 (2014) 181-187.

[6] M. León, S. Levcenko, R. Serna, G. Gurieva, A. Nateprov, J.M. Merino, E.J. Friedrich, U. Fillat, S. Schorr, E. Arushanov, Optical constants of Cu_2ZnGeS_4 bulk crystals, J. Appl. Phys. 108 (2010) 093502.

[7] C.J. Hages, S. Levcenco, C.K. Miskin, J.H. Alsmeier, D. Abou-Ras, R.G. Wilks, M. Bär, T. Unold, R. Agrawal, Improved performance of Ge-alloyed CZTGeSSe thin-film solar cells through control of elemental losses, Prog. Photovoltaics Res. Appl. 2013. DOI: 10-1002/pip.2442.

[8] T. Todorov, T. Gershon, O. Gunawan, C. Sturdevanta, S. Guha, Perovskite-kesterite monolithic tandem solar cells with high open-circuit voltage, Appl. Phys. Lett. 105 (2014) 173902-1-173902-4 (4 pages).

[9] B. Shin, O. Gunawan, Y. Zhu, N.A. Bojarczuk, S. J. Chey, S. Guha, Thin film solar cell with 8.4% power conversion efficiency using an earth-abundant Cu_2ZnSnS_4 absorber, Prog. Photovoltaics Res. Appl. 21 (2013) 72-76.

[10] T. Kato, H. Hiroi, N. Sakai, S. Muraoka, H. Sugimoto, Characterization of front and back interfaces on Cu_2ZnSnS_4 thin-film solar cells, in 27th EUPVSC, Frankfurt, 2012, pp. 2236-2239.

[11] I. Repins, C. Beall, N. Vora, C. DeHart, D. Kuciauskas, P. Dippo, B. To, J. Mann, W.C. Hsu, A. Goodrich, R. Noufi, Co-evaporated $Cu_2ZnSnSe_4$ films and devices, Sol. Energy Mater. Sol. Cells 101 (2012) 154-159.

[12] A. Redinger, M. Mousel, R.Djemour, K. Gütay, N. Valle, S. Siebentritt, $Cu_2ZnSnSe_4$ thin film solar cells produced via co-evaporation and annealing including a $SnSe_2$ capping layer, Prog. Photovoltaics Res.Appl. 22 (2014) 51-57.

[13] H. Katagiri, K. Jimbo, S. Yamada, T. Kamimura, W.S. Maw, T. Fukano, T. Ito, T. Motohiro, Enhanced conversion efficiencies of Cu_2ZnSnS_4-based thin film solar cells by using preferential etching technique, Appl. Phys. Express 1 (2008) 041201.

[14] J.J. Scragg, T. Ericson, X. Fontané, V. Izquierdo-Roca, A. Pérez-Rodríguez, T. Kubart, M. Edoff, C. Platzer-Björkman, Rapid annealing of reactively sputtered precursor for Cu_2ZnSnS_4 solar cells, Prog. Photovoltaics Res. Appl. 22 (2014) 10-17.

[15] Z. Shu, K. Sun, Z. Han, H. Cui, F. Liu, Y. Lai, J. Li, X. Hao, Y. Liu, M.A. Green, Fabrication of Cu_2ZnSnS_4 solar cells with 5.1% efficiency via thermal decomposition and reaction using a non-toxic sol-gel route, J. Mater. Chem. 2 (2014) 500-509.

[16] H. Araki, Y. Kubo, A. Mikaduki, K. Jimbo, W.S. Maw, H. Katagiri, M. Yamazaki, K. Oishi, A. Takeuchi, Preparation of Cu_2ZnSnS_4 thin films by sulfurizing electroplated precursors, Sol. Energy Mater. Sol. Cells 93 (2009) 996-999.

[17] I.V. Bodnar, Growth and properties of $CuAlS_{2x}Se_{2(1-x)}$ single crystals, Inorg. Mater. 38 (2002) 647-651.

[18] J.M. Merino, S. Mahanty, M. León, R. Díaz, F. Rueda, Structural characterization of $CuIn_2Se_{3.5}$, $CuIn_3Se_5$ and $CuIn_5Se_8$ compounds, Thin Solid Films 361-362 (2000) 70-73.

[19] R. Caballero, V. Izquierdo-Roca, J.M. Merino, E.J. Friedrich, A. Climent-Font, E. Saucedo, A. Pérez-Rodríguez, M. León, Cu_2ZnSnS_4 thin films grown by flash evaporation and subsequent annealing in Ar atmosphere, Thin Solid Films 535 (2013) 62-66.

[20] X. Fontané, L. Calvo-Barrio, V. Izquierdo-Roca, E. Saucedo, A. Pérez-Rodríguez, J.R. Morante, D.M. Berg, P.J. Dale, S. Siebentritt, In-depth resolved Raman scattering analysis for the identification of secondary phases: Characterization of Cu_2ZnSnS_4 layers for solar cell applications, Appl. Phys. Lett. 98 (2011) 181905.

[21] T.K. Todorov, J. Tang, S. Bag, O. Gunawan, T. Gokmen, Y. Zhu, D.B. Mitzi, Beyond 11% efficiency: Characteristics of state-of-the-art $Cu_2ZnSn(S,Se)_4$ solar cells, Adv. Energy Mater. 3 (2013) 34-38.

[22] J. Chen, W. Li, C. Yan, S. Huang, X. Hao, Studies of compositional dependent $Cu_2Zn(Ge_xSn_{1-x})S_4$ thin films prepared by sulfurizing sputtered metallic precursors, J.Alloys Compd. 2014. DOI: 10.1016/j.allcom.2014.09.097.

[23] A. Weber, R. Mainz, H.W. Schock, On the Sn loss from thin films of the material system Cu-Zn-Sn-S in high vacuum, J. Appl. Phys. 107 (2010) 013516-1-013516-5 (5 pages).

[24] R.E. Nikolaev, I.G. Vasilyeva, A new way of phase identification of $AgGaGeS_4.nGeS_2$ crystals, J. Solid State Chem. 203 (2013) 340-344.

[25] V. Piacente, S. Foglia, P. Scardala, Sublimation study of the tin sulphides SnS_2, Sn_2S_3 and SnS, J. Alloys Compd.117 (1991) 17-30.

[26] M. Guc, A.P. Litvinchuk, S. Levcenco, V. Izquierdo-Roca, X. Fontané, M.Ya. Valakh, E. Arushanov, A. Pérez-Rodríguez, Optical phonons in the wurtzstannite Cu_2ZnGeS_4 semiconductor: Polarized Raman spectroscopy and first-principle calculations, Phys. Rev. B 89 (2014) 205205.

[27] M. Dimitrievska, A. Fairbrother, X. Fontané, T. Jawhari, V. Izquierdo-Roca, E. Saucedo, A. Pérez-Rodríguez, Multiwavelength excitation Raman scattering study of polycrystalline kesterite Cu_2ZnSnS_4 thin films, Appl. Phys. Lett. 104 (2014) 021901.

[28] R. Caballero, E. Garcia-Llamas, J.M. Merino, M. León, I. Babichuk, V. Dzhagan, V. Strelchuk, M. Valakh, Non-stoichiomety effect and disorder in Cu2ZnSnS4 thin films obtained by flash evaporation: Raman scattering investigation, Acta Mater. 65 (2014) 412-417.

[29] X. Fontané, V. Izquierdo-Roca, E. Saucedo, S. Schorr, V.O. Yukhymchuk, M.Ya. Valakh, A. Pérez-Rodríguez, J.R. Morante, Vibrational properties of stannite and kesterite type compounds: Raman scattering analysis of $Cu_2(Fe,Zn)SnS_4$, J. Alloys Compd. 539 (2012) 190-194.

[30] M. Guc, V. Izquierdo-Roca, A. Pérez-Rodríguez, G. Gurieva, S. Levcenko, S. Schorr, E. Arushanov, Raman spectra of wurtzstannite quaternary compounds, Phys. Status Solidi C 10 (2013) 1075-1078.

[31] M. Himmrich, H. Haeuseler, Far infrared studies on stannite and wurtzstannite type compounds, Spectrochimica Acta 47A (1991) 933-942.

[32] K. Zhang, Z. Su, L. Zhao, C. Yan, F. Liu, H. Cui, X. Hao, Y. Liu, Improving the conversion efficency of Cu_2ZnSnS_4 solar cell by low pressure sulfurization, Appl. Phys. Lett. 104 (2014)141101-1-141101-4 (4 pages).

[33] R. Caballero, C.A. Kaufmann, V. Efimova, T. Rissom, V. Hoffmann, H.W. Schock, Investigation of $Cu(In,Ga)Se_2$ thin-film formation during the multi-stage co-evaporation process, Prog.Photovoltaics Res. Appl. 21 (2013) 30-46.

[34] S.H. Wei, S.B. Zhang, A. Zunger, Effects of Na on the electrical and structural properties of $CuInSe_2$, J. Appl. Phys. 85 (1999), 7214.

[35] F. Pianezzi, P. Reinhard, A. Chirila, B. Bissing, S. Nishiwaki, S. Buecheler, A.N. Tiwari, Unveilling the effects of post-deposition treatment with different alkaline elements on the electronic properties of CIGS thin film solar cells, Phys. Chem. Chem. Phys. 16 (2014) 8843-8851.

[36] C.M. Sutter-Fella, J.A. Stückelberger, H. Hagendorfer, F. La Mattina, L. Kranz, S. Nishiwaki, A.R. Uhl, Y.E. Romanyuk, A.N. Tiwari, Sodium assited sintering of chalcogenides and its application to solution processed $Cu_2ZnSn(S,Se)_4$ thin film solar cells, Chem.Mater. 26 (2014) 1420-1425.

[37] H. Zhou, T-B Song, W-C Hsu, S. Luo, S. ye, H-S Duan, C-J Hsu, W. Yang, Y. Yang, Rational defect passivation of $Cu_2ZnSn(S,Se)_4$ photovoltaics with solution-processed Cu_2ZnSnS_4:Na nanocrystals, J. Am. Chem. Soc. 135 (2013) 15998-16001.

[38] J.V. Li, D. Kuciauskas, M.R. Young, I.L. Repins, Effects of sodium incorporation in co-evaporated $Cu_2ZnSnSe_4$ thin-film solar cells, Appl. Phys. Lett. 102 (2013) 163905.

[39] A.M. Gabor, J.R. Tuttle, D.S. Albin, M.A. Contreras, R. Noufi, A.M. Hermann, High-efficiency $CuIn_xGa_{1-x}Se_2$ solar cells made from $(In_xGa_{1-x})_2Se_3$ precursor films, Appl. Phys. Lett. 65 (1994) 198-200.

[40] A. Chirila, S. Buecheler, F. Pianezzi, P. Bloesch, Ch. Gretener, A.R. Uhl, C. Fella, L. Kranz, J. Perrenoud, S. Seyrling, R. Verma, S. Nishiwaki, Y. E. Romanyuk, G. Bilger, A.N. Tiwari, Highly efficient $Cu(In,Ga)Se_2$ solar cells grown on flexible polymer films, Nat. Mater. 10 (2011) 857-861.

[41] C. Persson, Electronic and optical properties of Cu_2ZnSnS_4 and $Cu_2ZnSnSe_4$, J. Appl. Phys. 107 (2010) 053710.

[42] S. Siebetritt, S. Schorr, Kesterites- a challenging material for solar cells, Prog. Photovoltaics Res. Appl. 2012, DOI: 10.1002/pip.2156.

[43] A. Fairbrother, V. Izquierdo-Roca, X. Fontané, M. Ibáñez, A. Cabot, E. Saucedo, A. Pérez-Rodríguez, ZnS grain size effects on near-resonant Raman scattering: optical non-destructive grain size estimation, Cryst. Energ. Comm. 16 (2014) 4120-4125.

[44] A. Fairbrother, E. García-Hemme, V. Izquierdo-Roca, X. Fontané, F.A. Pulgarín-Agudelo, O. Vigil-Galán, A. Pérez-Rodríguez, E. Saucedo, Development of a selective

chemical etch to improve the conversión efficiency of Zn-rich Cu_2ZnSnS_4 solar cells, J. Am.Chem. Soc. 2012, DOI: 10.1021/ja301373e.

[45] D. Abou-Ras, R. Caballero, C.A. Kaufmann, M. Nichterwitz, K. Sakurai, S. Schorr, T. Unold, H.W. Schock, Impact of the Ga concentration on the microstructure of $CuIn_{1-x}Ga_xSe_2$, Rapid Res. Lett. 2 (2008) 135-137.

Figure Captions

Figure 1. GIXRD spectra of as-evaporated samples by using grazing incidence angle of 4º. JCPDS references of CZTS, CTGS, ZnS and Cu_2S are shown for comparison.

Figure 2. GIXRD spectra of as-evaporated samples coming from process Flash 1 after different thermal treatments. Grazing incidence angle of 4º is used. JDPDS references of CZTS, CZTGS and SnS are also shown for comparison.

Figure 3. Raman spectra of as-evaporated samples coming from process Flash 1 after thermal treatment (a) TT1, (b) TT3 and (c) TT4. An excitation wavelength of 514.5 nm is used. Lorentzian fits and linear background were carried out to determine the Raman peaks position. Th inset of Figure 3.b. shows the Raman spectra of the sample after thermal treatment TT3 measured using excitation by light at 325 nm wavelength. The inset of Figure 3.c. displays the comparison of the Raman spectra of the different samples.

Figure 4. Cross-sectional SEM micrographs of the CZTGS/Mo/glass structure and surface morphology of samples coming from process Flash 1 after thermal treatment (a) TT1, (b) TT2, (c) TT34, (d) TT4; from process Flash 2 after thermal treatment (e) TT1, (f) TT2, (g) TT3, (h) TT5; from process Flash 3 after thermal treatment (i) TT1, (k) TT3 and (l) TT5. Figure 4.j. shows the EDX elemental mapping of the sample represented in (f). Insets of Figure 4.a. – 4.e. and 4.f – 4.l. show the surface morphology of the films using x 5 K and x 50 K amplifications respectively.

Figure 5. GDOES depth profiles of the films coming from process Flash 1 after thermal treatments TT1, TT3 and TT4.

Figure 6. (a) GIXRD spectra using grazing incidence angles of 0.25º, 2º and 4º of the sample coming from Flash 2 after thermal treatment TT1. (b) Raman spectra measured using 325 nm and (c) Area ratio of LO and LO2 or LO3 Raman peaks of the samples coming from Flash 2 after different thermal treatments.

Figure 7. (a) GIXRD spectra, (b) Raman spectra at 532 nm and (c) 325 nm excitation wavelengths of the as-evaporated samples coming from process Flash 3 before and after different thermal treatments. In (a) JCPDS references of CZTS, CTGS, ZnS and Cu_2S are shown for comparison. Insets in (b) and (c) display the Raman spectra in the range 320-370 cm^{-1}.

Table I. Composition of the different deposition processes.

	Cu(at%)	Zn(at%)	Sn(at%)	Ge(at%)	S(at%)	Cu/(Zn+IV)	x	Zn/IV	S/M
Bulk	21.66	17.03	4.86	5.59	50.87	0.79	0.54	1.63	1.04
Flash 1	18.68	8.42	10.52	8.81	53.57	0.67	0.46	0.44	1.15
Flash 2	16.08	16.25	7.20	7.00	53.47	0.53	0.49	1.14	1.15
Flash 3	23.52	15.78	8.70	2.05	49.94	0.89	0.19	1.47	1.00

Note: Flash 1: $T_{substrate}$ = 100º C; Flash 2: $T_{substrate}$ = 100º C, 50% extra of ZnS; Flash 3: $T_{substrate}$ = 350º C, 50% extra of ZnS.

M = Cu + Zn + Sn + Ge; IV = Sn + Ge.

Table II. Thermal treatments of the as-evaporated thin films. All the treatments were carried out by using a heating-rate = 20º C/min and at maximum temperature of 550º C with the exception of TT5 performed at 500º C

	Cu(at%)	Zn(at%)	Sn(at%)	Ge(at%)	S(at%)	Cu/(Zn+IV)	x	Zn/IV	S/M
Flash 1 ($T_{substrate}$ = 100º C)									
TT1	22.50	10.16	12.64	2.10	52.60	0.90	0.14	0.69	1.11
TT2	21.90	10.44	11.70	2.38	53.57	0.89	0.17	0.74	1.15
TT3	22.23	10.15	11.33	3.04	53.25	0.91	0.21	0.71	1.14
TT4	22.60	10.43	11.81	1.91	53.26	0.94	0.14	0.76	1.14
Flash 2 ($T_{substrate}$ = 100º C, 50 % extra of ZnS)									
TT1	18.94	11.74	7.94	2.52	52.86	0.67	0.24	1.70	1.12
TT2	19.10	16.89	8.11	3.39	52.52	0.67	0.29	1.47	1.11
TT3	19.33	16.07	8.17	3.33	53.10	0.70	0.29	1.40	1.13
TT5	18.67	16.98	7.75	4.53	52.07	0.64	0.37	1.38	1.09
Flash 3 ($T_{substrate}$ = 350º C, 50 % extra of ZnS)									
TT1	23.05	14.57	9.89	2.11	50.38	0.87	0.18	1.21	1.02
TT3	20.78	12.47	9.83	3.41	53.51	0.81	0.26	0.94	1.15

Note: TT1: P = 9.5 x 10^4 Pa, t = 30 min; TT2: P = 9.5 x 10^4 Pa, t = 60 min; TT3: P = 4.5 x 10^4 Pa, t = 30 min; TT4: P = 4.5 x 10^4 Pa, t = 60 min; TT5: P = 9.5 x 10^4 Pa, t = 30 min, T = 500º C.

Figure 1

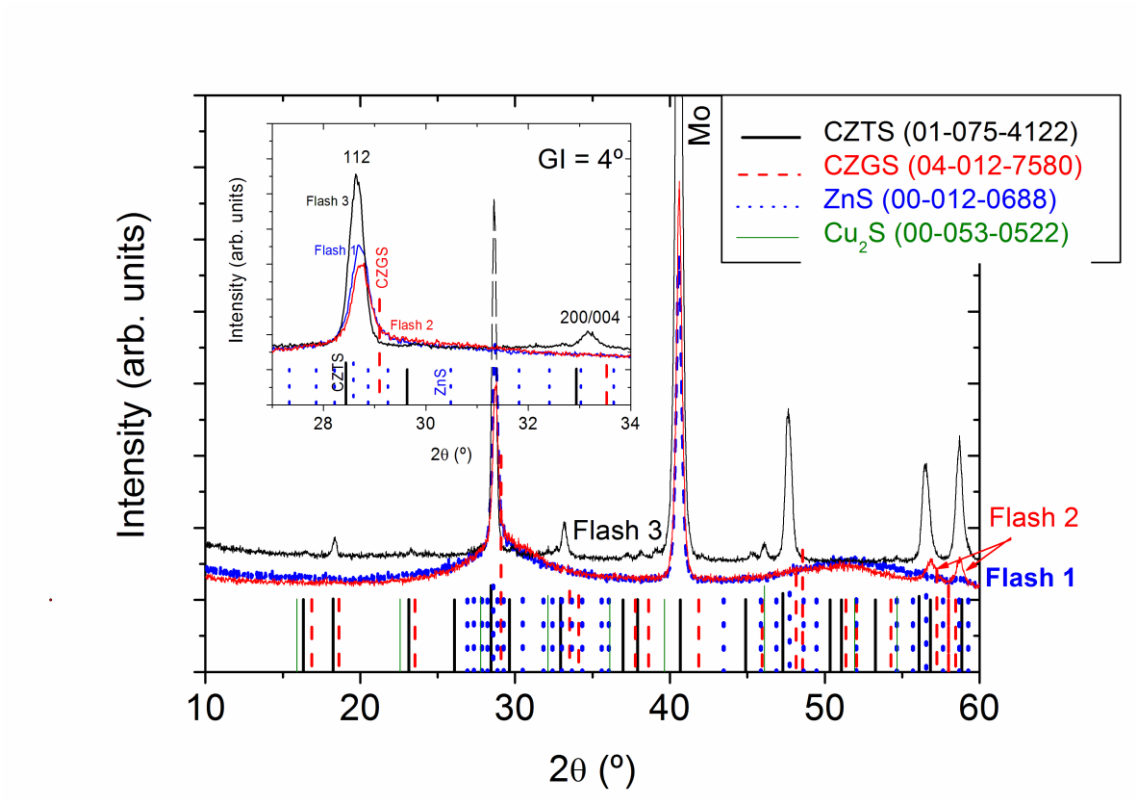
Intensity (arb. units)
2θ (°)
CZTS (01-075-4122)
CZGS (04-012-7580)
ZnS (00-012-0688)
Cu2S (00-053-0522)
Mo
Flash 3
Flash 2
Flash 1
GI = 4°
112
200/004
CZTS
ZnS
CZGS

Figure 2

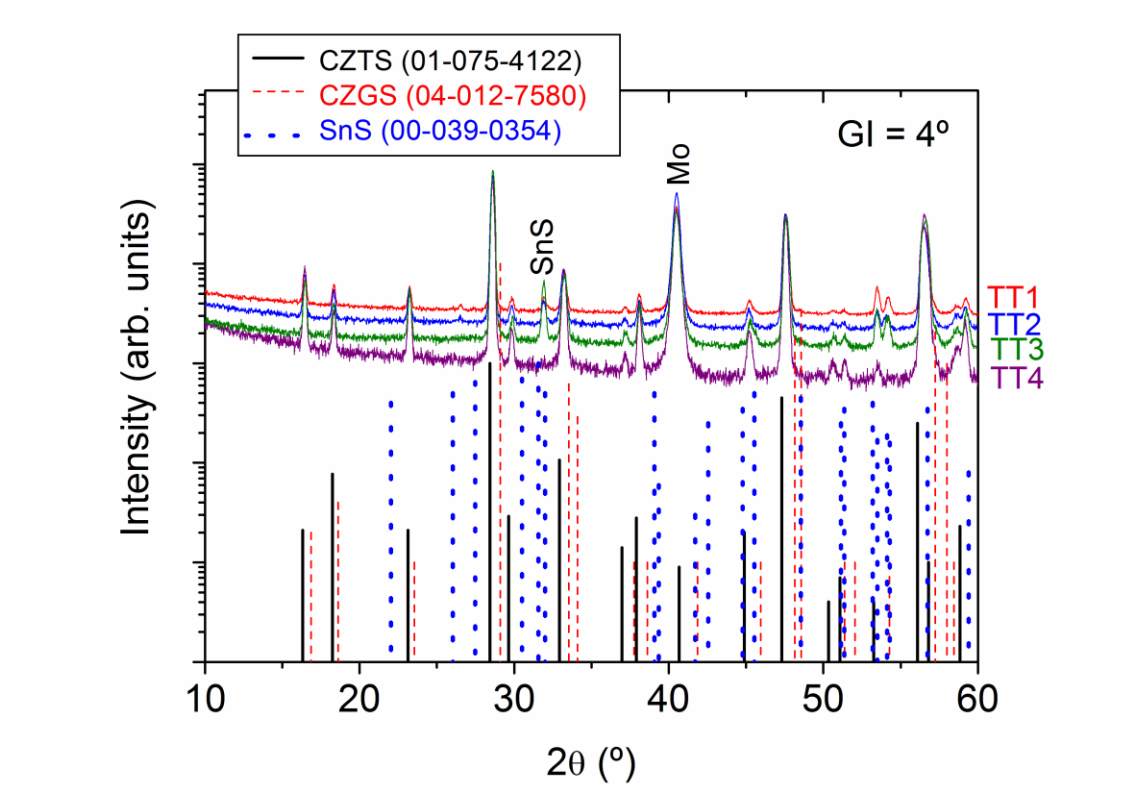
CZTS (01-075-4122)
CZGS (04-012-7580)
SnS (00-039-0354)
GI = 4º
SnS
Mo
TT1
TT2
TT3
TT4
Intensity (arb. units)
10
20
30
40
50
60
2θ (º)

Figure 3

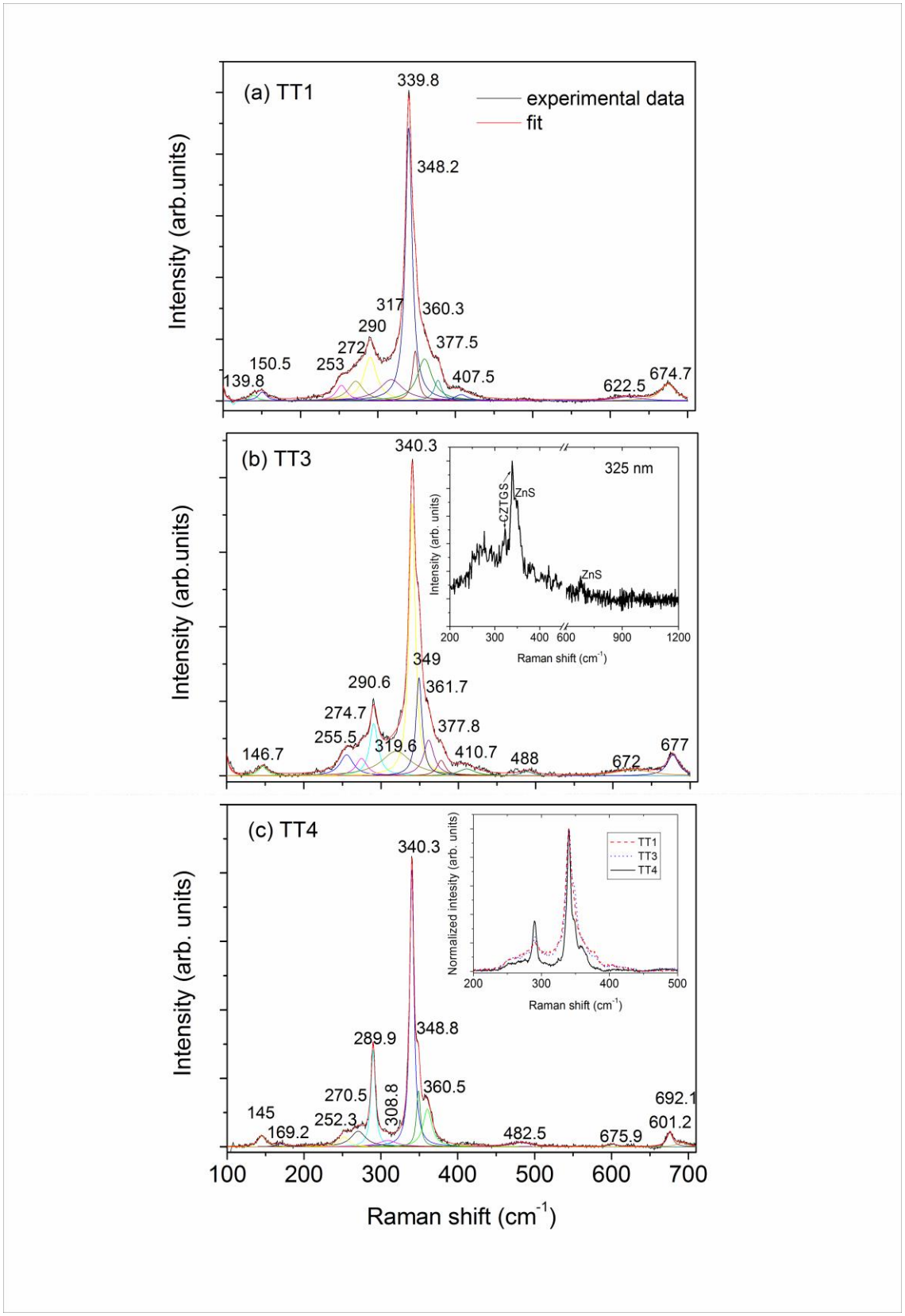
(a) TT1
experimental data
fit
339.8
348.2
317
360.3
290
272
377.5
253
150.5
139.8
407.5
622.5
674.7
Intensity (arb.units)
(b) TT3
340.3
325 nm
CZTGS
ZnS
ZnS
Intensity (arb. units)
Raman shift (cm-1)
349
290.6
361.7
274.7
377.8
255.5
319.6
410.7
488
672
677
146.7
Intensity (arb.units)
(c) TT4
340.3
Normalized intesity (arb. units)
TT1
TT3
TT4
Raman shift (cm-1)
289.9
348.8
270.5
360.5
308.8
692.1
145
252.3
601.2
169.2
482.5
675.9
Intensity (arb. units)
100
200
300
400
500
600
700
Raman shift (cm-1)

Figure 4

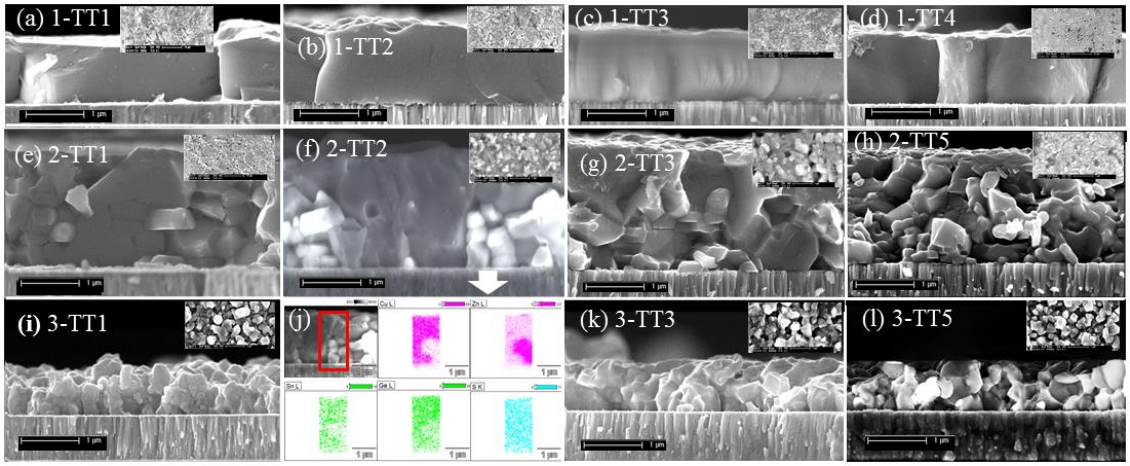
(a) 1-TT1
(b) 1-TT2
(c) 1-TT3
(d) 1-TT4
(e) 2-TT1
(f) 2-TT2
(g) 2-TT3
(h) 2-TT5
(i) 3-TT1
(j)
(k) 3-TT3
(l) 3-TT5

Figure 5

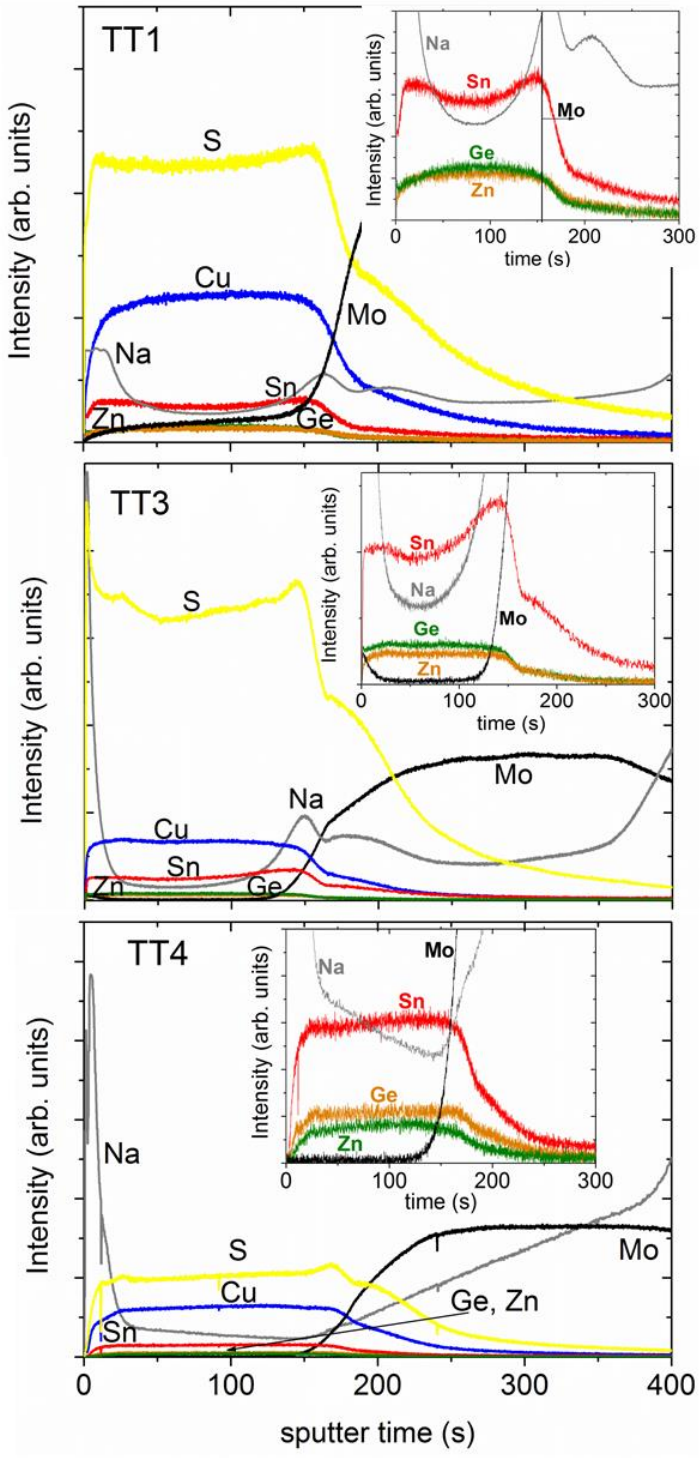
TT1
S
Cu
Mo
Na
Sn
Zn
Ge
Intensity (arb. units)
Na
Sn
Mo
Ge
Zn
0
100
200
300
time (s)
TT3
S
Na
Mo
Cu
Sn
Zn
Ge
TT4
Na
S
Cu
Sn
Mo
Ge, Zn
0
100
200
300
400
sputter time (s)

Figure 6a

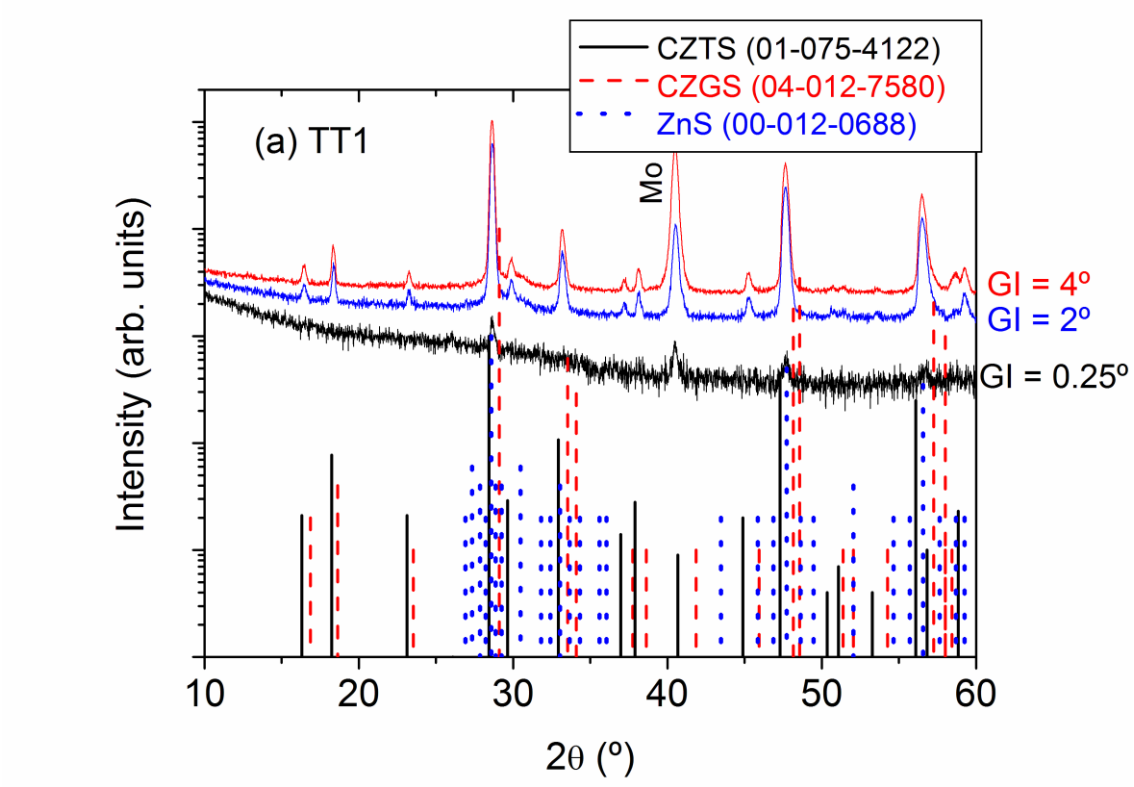
CZTS (01-075-4122)
CZGS (04-012-7580)
ZnS (00-012-0688)
(a) TT1
Mo
GI = 4º
GI = 2º
GI = 0.25º
Intensity (arb. units)
10
20
30
40
50
60
2θ (º)

Figure 6b

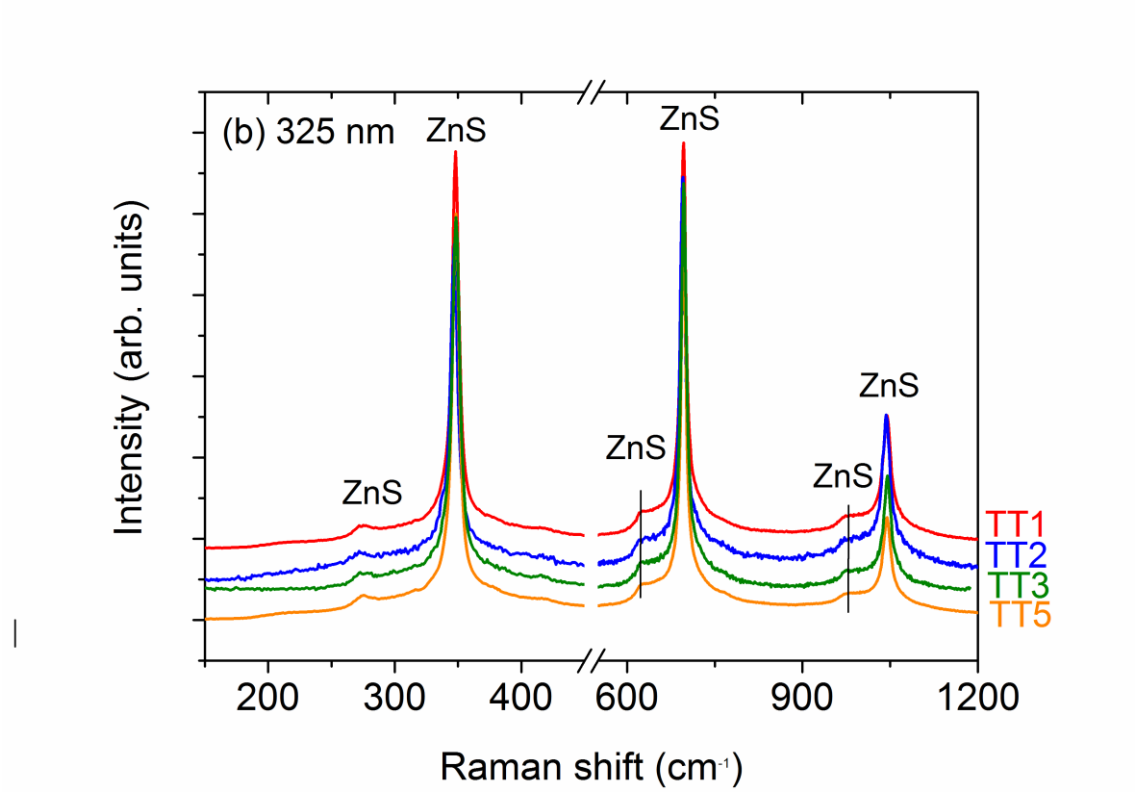
(b) 325 nm
ZnS
ZnS
ZnS
ZnS
ZnS
ZnS
TT1
TT2
TT3
TT5
Intensity (arb. units)
200
300
400
600
900
1200
Raman shift (cm-1)

Figure 6c

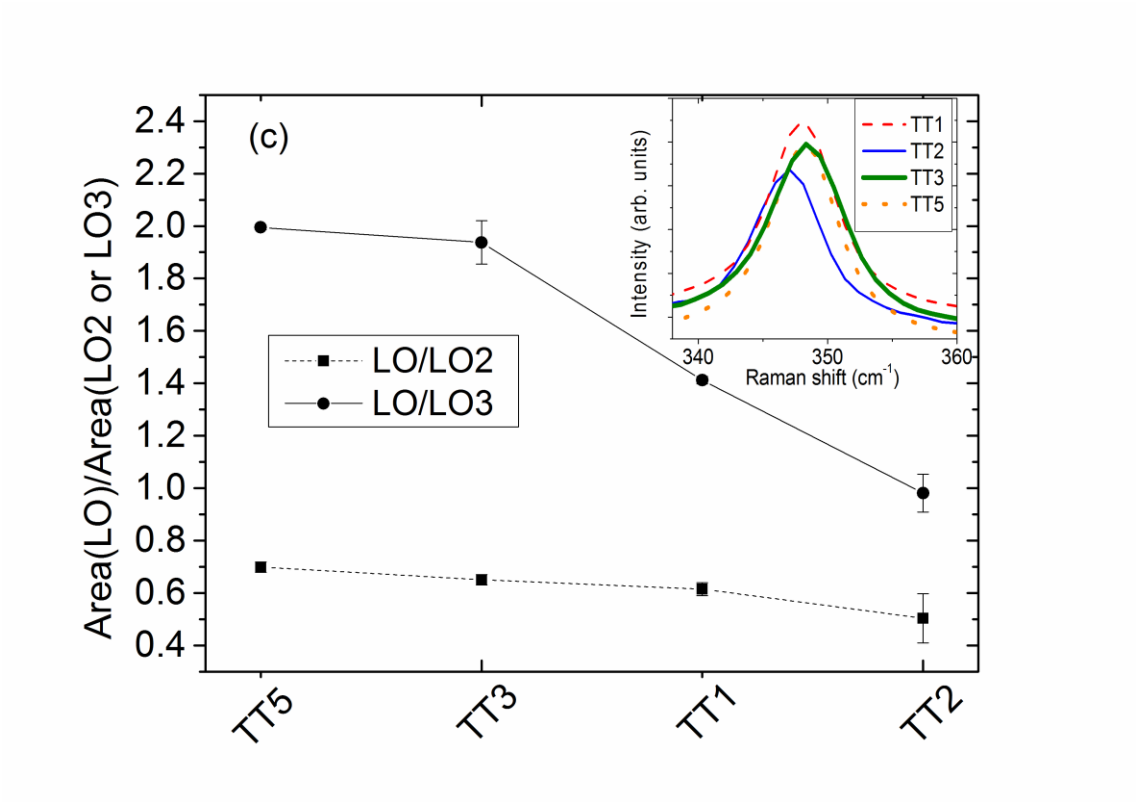
(c)
Area(LO)/Area(LO2 or LO3)
2.4
2.2
2.0
1.8
1.6
1.4
1.2
1.0
0.8
0.6
0.4
LO/LO2
LO/LO3
TT5
TT3
TT1
TT2
Intensity (arb. units)
TT1
TT2
TT3
TT5
340
350
360
Raman shift (cm-1)

Figure 7a

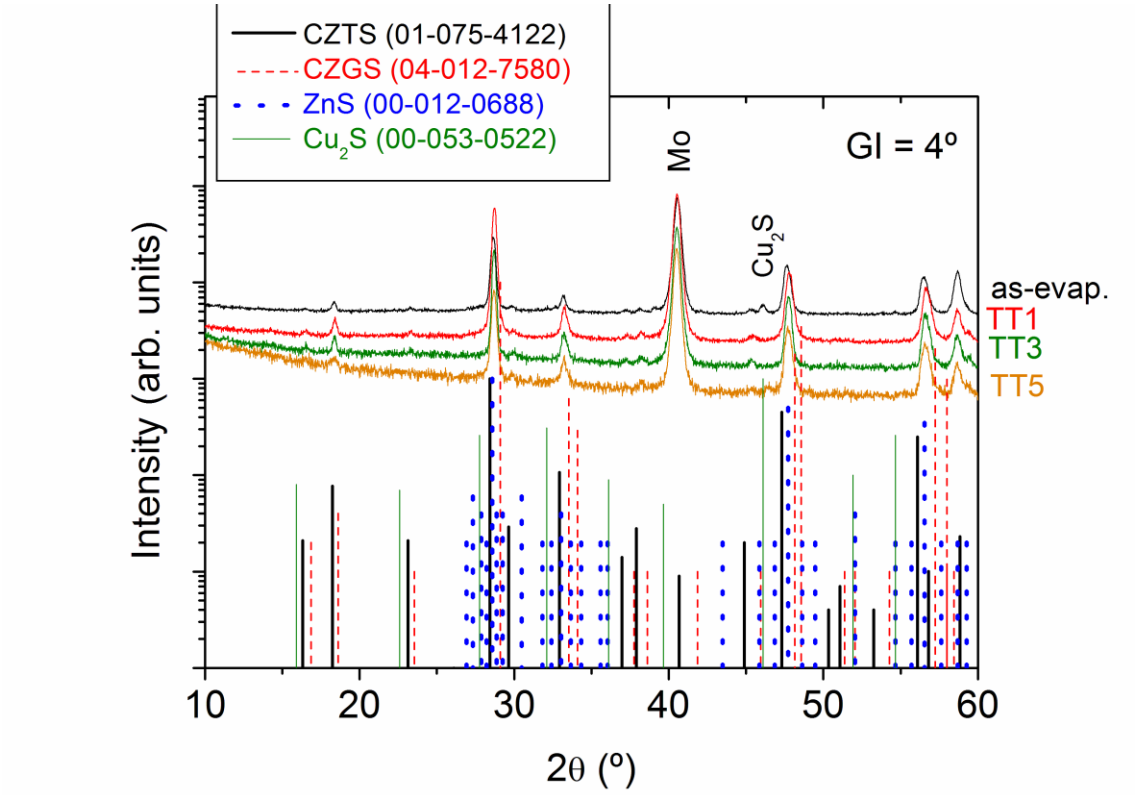
CZTS (01-075-4122)
CZGS (04-012-7580)
ZnS (00-012-0688)
Cu2S (00-053-0522)
Mo
Cu2S
GI = 4º
as-evap.
TT1
TT3
TT5
Intensity (arb. units)
10
20
30
40
50
60
2θ (º)

Figure 7b

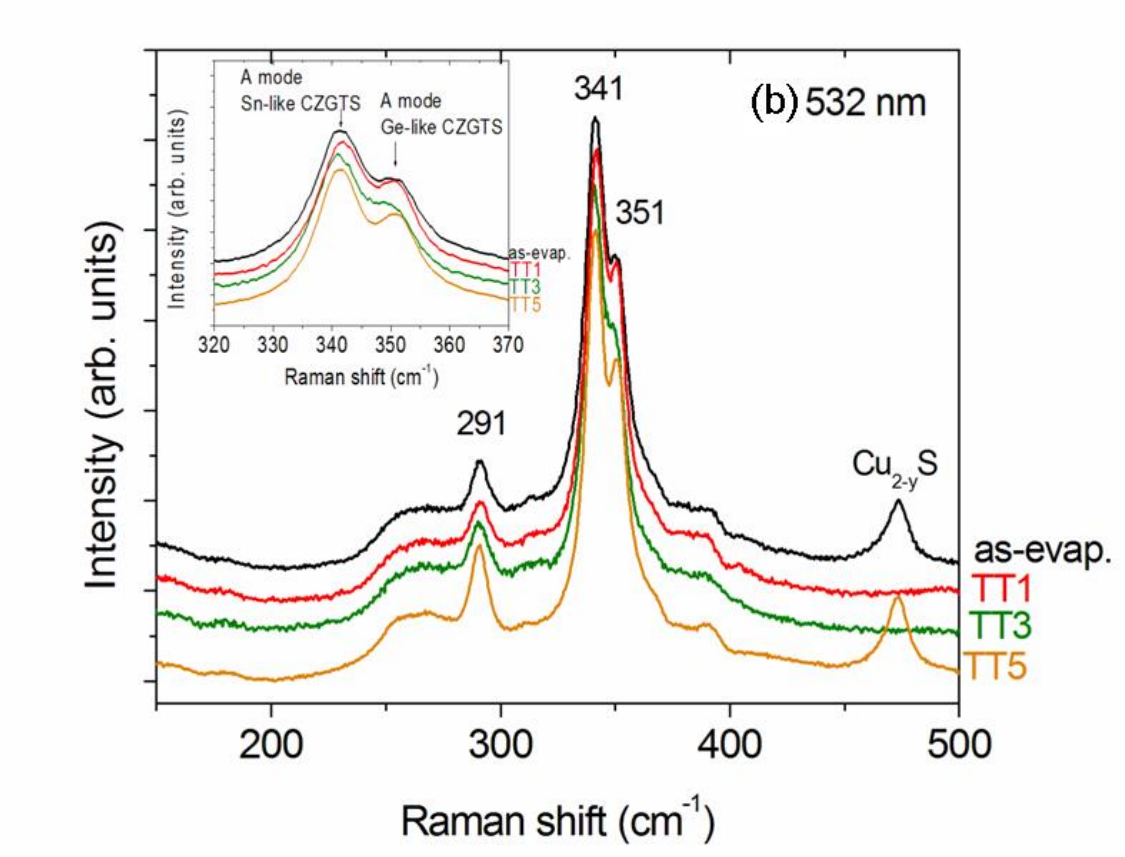
(b) 532 nm
341
351
291
Cu2-yS
as-evap.
TT1
TT3
TT5
Intensity (arb. units)
Raman shift (cm-1)
200
300
400
500
A mode
Sn-like CZGTS
A mode
Ge-like CZGTS
320
330
340
350
360
370

Figure 7c

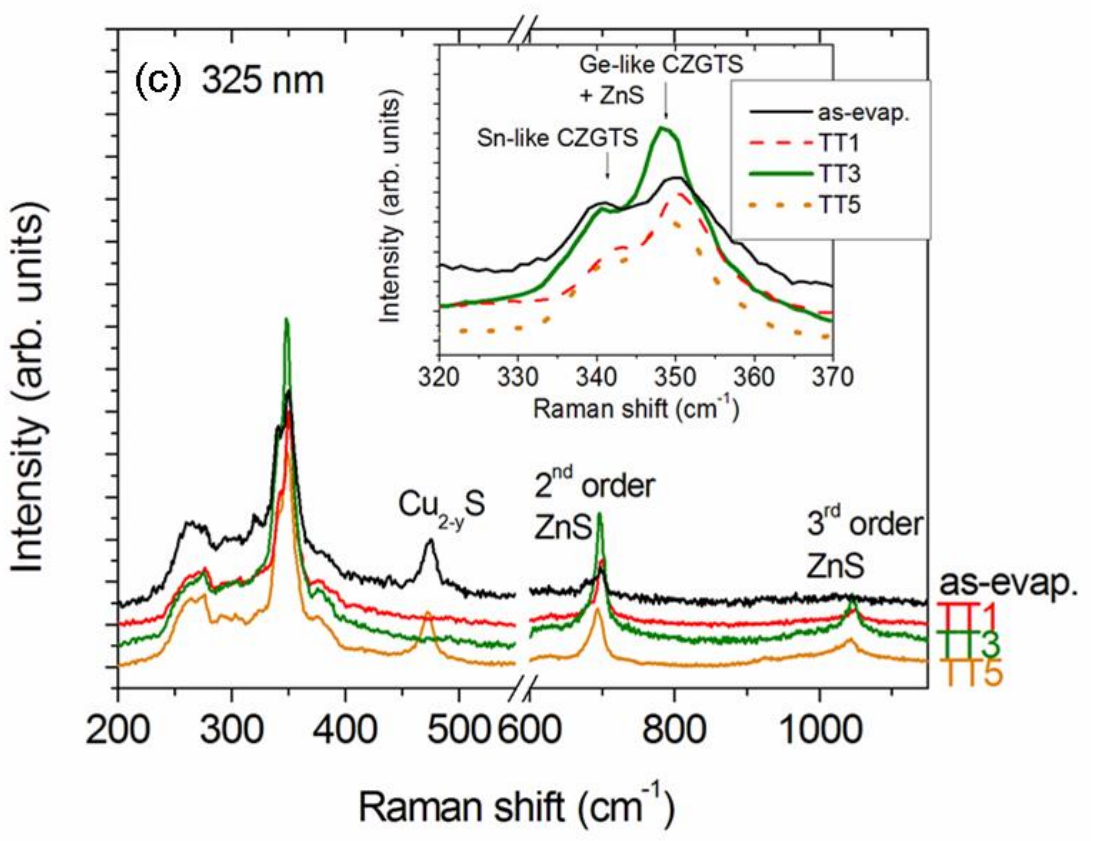
(c) 325 nm
Ge-like CZGTS
+ ZnS
Sn-like CZGTS
as-evap.
TT1
TT3
TT5
Intensity (arb. units)
320
330
340
350
360
370
Raman shift (cm-1)
Cu2-yS
2nd order
ZnS
3rd order
ZnS
as-evap.
TT1
TT3
TT5
Intensity (arb. units)
200
300
400
500
600
800
1000
Raman shift (cm-1)